A nonstandard multigrid method with flexible multiple semicoarsening for the numerical solution of the pressure equation in a Navier–Stokes solver

Jean Piquet [a,*] and Xavier Vasseur [b]

[a] *Ecole Centrale de Nantes, Laboratoire de Mécanique des Fluides UMR 6598, 1, rue de la Noë, B.P. 92101, F-44321 Nantes Cedex 3, France*

[b] *Laboratoire d'Informatique et de Mécanique pour les Sciences de l'Ingénieur UPR 3251, B.P. 133, F-91403 Orsay Cedex, France*

Numerical methods for the incompressible Reynolds-averaged Navier–Stokes equations discretized by finite difference techniques on collocated cell-centered structured grids are considered in this paper. A widespread solution method to solve the pressure–velocity coupling problem is to use a segregated approach, in which the computational work is deeply controlled by the solution of the pressure problem. This pressure equation is an elliptic partial differential equation with possibly discontinuous or anisotropic coeffficients. The resulting singular linear system needs efficient solution strategies especially for 3-dimensional applications. A robust method (close to MG-S [22,34]) combining multiple cell-centered semicoarsening strategies, matrix-independent transfer operators, Galerkin coarse grid approximation is therefore designed. This strategy is both evaluated as a solver or as a preconditioner for Krylov subspace methods on various 2- or 3-dimensional fluid flow problems. The robustness of this method is shown.

Keywords: multigrid method, Krylov subspace method, incompressible Navier–Stokes equations, semicoarsening, robustness

AMS subject classification: 65F10, 65N55, 76D05, 76M20

1. Introduction

The numerical solution of 3-dimensional linear elliptic partial differential equations with possibly discontinuous or anisotropic coefficients is of relevant importance in many fields of computational fluid dynamics (CFD) (e.g., oil reservoir simulation, environmental remediation, direct numerical simulation of turbulent fluid flows, etc.). The common crucial key point of all these applications in terms of computational work is to dispose of an efficient and robust 3-dimensional elliptic solver, if possible, adapted to recent hardware computer technologies (parallel architectures). Multigrid methods are known to have optimal complexity, e.g., O(N) operations are needed to solve a linear or nonlinear system of N unknowns. Nowadays, the application of the multi-

* Corresponding author.

© J.C. Baltzer AG, Science Publishers

grid theory in computational fluid dynamics becomes more and more a maturing field. Nevertheless, there still exist some bottlenecks inhibiting full efficiency (see [4] for a review). Our previous work [25] described a robust linear multigrid method combining incomplete decomposition method as a smoother with an algebraic construction of the coarse grid operators by means of the Galerkin approximation [2,11,36]. An extensive performance comparison between various linear solvers (preconditioned Krylov subspace versus multigrid methods) on various fluid flow problems for 3-dimensional applications has been proposed therein. Multigrid preconditioned BiCGSTAB [30] was found to be the most efficient solution method either on a workstation or on a vector machine (CRAY 98). Nevertheless the high recursivity of incomplete decomposition methods in the smoothing steps would yield a poor parallel efficiency, motivating the search for new multigrid methods. Thus, the goal of this paper is to present the computational issues concerning the design of a robust multigrid-based solver with expected good efficiency on a parallel platform. As in [25], the performances of the proposed solution method will be evaluated in the framework of incompressible viscous fluid flow simulation around moderately complex geometries by solving the pressure problem. The parallel implementations are not considered in this paper, only the robustness of MG-S will be examined.

It is widely accepted that a mandatory key to achieve robustness for the solution of 3-dimensional elliptic problems in standard multigrids is to use alternating plane smoothers [1,14,29]. Thus, in every plane, a 2-dimensional sparse linear system has to be solved or approximately solved, this is expensive and prone to a suboptimal parallel efficiency (for anisotropic problems, an increase in plane smoothing iterations is generally found in several planes, leading to unbalanced workload on Multiple Instruction Multiple Data (MIMD) machines). Alternatives are therefore needed. To yield simultaneously parallelism and robustness, nonstandard multigrid methods based on semicoarsening (coarsening in one direction) or multiple semicoarsening have to be considered. This framework generally involves a combination of local smoothers and of robust coarse-grid corrections based on semicoarsened grids. Since the pioneering work of Mulder [19], semicoarsening has become a frequently adopted technique still currently investigated for calculations either on structured or non-structured meshes for elliptic or non-elliptic problems [8,17]. Following recent work of Oosterlee [22] and Washio and Oosterlee [33,34], a nonstandard multigrid method with flexible coarsening called MultiGrid as a Smoother (MG-S) is adopted here to benefit from its high robustness. Nevertheless some difficulties in MG-S pointed by Oosterlee and Washio concerned the construction of the discrete operators along the standard coarse and semicoarsened grids. The use of *matrix-dependent* transfer operators (de Zeeuw's [7] and Dendy's [5] prolongation weights) with the Galerkin approximation in a *vertex-centered* formulation led for some difficult problems to bad properties for coarse or semicoarsened grid operators, that might even cause divergence of the relaxation process. A numerical cure – lumping strategy – was proposed in [34] to overcome this difficulty. Here this work aims to present another approach for the construction of the coarse and semicoarsened grid operators. The main idea consists in using the Galerkin ap-

proximation with *matrix-independent* transfer operators in a *cell-centered* formulation (italic terms refer to the main differences with [34]). The robustness and ability to treat difficult linear problems with such a Galerkin approximation have been proved in [15,16,35] for standard multigrids. The present work will propose a generalization for a nonstandard multigrid with semicoarsening that always preserves the M-matrix property for the considered problem.

This paper is organized as follows. Section 2 introduces the numerical background of this study. Since the basis of the 3-dimensional solution method is a 2-dimensional nonstandard multigrid solver, a 2-dimensional nonstandard multigrid method with flexible multiple semicoarsening will be presented in section 3. The features of the 3-dimensional variant will then be presented and discussed. Section 4 will summarize various numerical experiments on 2- or 3-dimensional model and fluid flow problems. Finally observations are made and conclusions are drawn in section 5.

2. The numerical background

In this section, the numerical background of this study is introduced. The elliptic partial differential equation to be solved at each nonlinear iteration is presented.

2.1. The pressure problem and some notations

The pressure problem. The numerical solution of the Navier–Stokes equations for an incompressible viscous fluid around moderately complex geometries has given rise to numerous methods in the last thirty years. The main difficulty lies in the lack of any pressure term in the continuity equation, causing the occurrence of a zero block diagonal term in the linearized Navier–Stokes system gathering velocity and pressure variables. Among various strategies, one classical approach to remedy this bottleneck consists in using a "pressure-correction" method [6]. At each nonlinear iteration, a pressure equation has to be solved to yield a divergence-free velocity field after the correction step. This elliptic partial differential equation to be solved on the d-dimensional computational domain $\Omega = [0,1] \times \cdots \times [0,1]$ of basis $(\xi^1, \ldots, \xi^d)$ may be written as follows:

$$-\frac{\partial}{\partial \xi^i}\left(J g^{ii} \frac{C_{nn} R_{\text{eff}}}{(1 + e_1 C_{nn})} \frac{\partial P}{\partial \xi^i} \right) = -\frac{\partial}{\partial \xi^i}\left(b^i_j U^\star_j \right) + \frac{\partial}{\partial \xi^i}\left(J g^{ij}_{i \neq j} \frac{C_{nn} R_{\text{eff}}}{(1 + e_1 C_{nn})} \frac{\partial P}{\partial \xi^j} \right) \quad (1)$$

with Neumann-type boundary conditions (where n denotes the outward normal):

$$\left.\frac{\partial P}{\partial n}\right|_{\xi^1=0,\ldots,\xi^d} = \left.\frac{\partial P}{\partial n}\right|_{\xi^1,\ldots,\xi^d=0} = 0, \quad (2)$$

$$\left.\frac{\partial P}{\partial n}\right|_{\xi^1=1,\ldots,\xi^d} = \left.\frac{\partial P}{\partial n}\right|_{\xi^1,\ldots,\xi^d=1} = 0. \quad (3)$$

In equation (1) where there is a sum over the i and j indices, the geometry-induced parameters J, g^{ij} and b^i_j are respectively the Jacobian, the contravariant component

of the metric tensor and the components of the contravariant area vector b^i, due to a partial coordinate transformation between physical and computational spaces. The C_{nn} factors are the convection–diffusion central coefficients for velocity variables, $U_j^\star$ denote components of a guessed velocity field, e_1 – a dimensionless paramater akin to a false time-step and, finally, R_{eff} – the effective Reynolds number defined by

$$\frac{1}{R_{\text{eff}}} = \frac{1}{Re} + \nu_{\text{T}}, \tag{4}$$

where ν_{T} is the turbulent viscosity and *Re* the Reynolds number.

Some notations. Throughout this study, the resulting pressure linear system is denoted $\mathbf{A}\phi = b$. The following notations for the structure of the pressure operator **A** are adopted for 2-dimensional applications:

$$[\mathbf{A}] = \begin{bmatrix} a_7 & a_8 & a_9 \\ a_4 & a_5 & a_6 \\ a_1 & a_2 & a_3 \end{bmatrix}. \tag{5}$$

Thus, the discrete form of $\mathbf{A}\phi = b$ is:

$$\begin{aligned} &a_1\phi_{i-1,j-1} + a_2\phi_{i,j-1} + a_3\phi_{i+1,j-1} + a_4\phi_{i-1,j} + a_5\phi_{i,j} + a_6\phi_{i+1,j} \\ &\quad + a_7\phi_{i-1,j+1} + a_8\phi_{i,j+1} + a_9\phi_{i+1,j+1} = b_{i,j}. \end{aligned} \tag{6}$$

For 3-dimensional applications, the corresponding structure is denoted as follows:

$$\begin{aligned} [\mathbf{A}]^{-1} &= \begin{bmatrix} a_{16} & a_{17} & a_{18} \\ a_{13} & a_{14} & a_{15} \\ a_{10} & a_{11} & a_{12} \end{bmatrix}, \qquad [\mathbf{A}]^{0} = \begin{bmatrix} a_7 & a_8 & a_9 \\ a_4 & a_5 & a_6 \\ a_1 & a_2 & a_3 \end{bmatrix}, \\ [\mathbf{A}]^{+1} &= \begin{bmatrix} a_{25} & a_{26} & a_{27} \\ a_{22} & a_{23} & a_{24} \\ a_{19} & a_{20} & a_{21} \end{bmatrix}, \end{aligned} \tag{7}$$

where $[\mathbf{A}]^{\mathrm{i}z}$ denotes the stencil of the operator in the plane $k + \mathrm{i}z$.

Properties of the pressure operator. After discretization of the pressure problem (1)–(3), **A** is a singular symmetric M-matrix [31]. Its one-dimensional nullspace is the span of the unitary vector e such as $e^{\text{T}} = (1, \ldots, 1)$. Second-order central differencing leads to a sparse matrix with a 5 or 7 point structure, respectively, in two dimensions:

$$[\mathbf{A}] = \begin{bmatrix} 0 & a_8 & 0 \\ a_4 & a_5 & a_6 \\ 0 & a_2 & 0 \end{bmatrix} \tag{8}$$

and in three dimensions:

$$[\mathbf{A}]^{-1} = \begin{bmatrix} 0 & 0 & 0 \\ 0 & a_{14} & 0 \\ 0 & 0 & 0 \end{bmatrix}, \qquad [\mathbf{A}]^{0} = \begin{bmatrix} 0 & a_8 & 0 \\ a_4 & a_5 & a_6 \\ 0 & a_2 & 0 \end{bmatrix}, \qquad [\mathbf{A}]^{+1} = \begin{bmatrix} 0 & 0 & 0 \\ 0 & a_{23} & 0 \\ 0 & 0 & 0 \end{bmatrix}. \tag{9}$$

Goal of this study. The solution of this equation requires a fairly robust and efficient solver especially for 3-dimensional applications, where the conditioning of this system is known to be very bad. Besides the large number of unknowns, the bad conditioning is primarily caused by the strong anisotropies in the pressure operator; this in turn is due to a combination of both various geometry-induced influence factors (such as cells with high aspect ratio, non-orthogonality, strong curvatures of the mesh lines) and anisotropies in the flow affecting the coefficients C_{nn}. In a previous work [25], a standard geometric multigrid method has been presented to solve efficiently this pressure linear system. Its main features were cell-centered coarsening [36], Galerkin coarse-grid approximation [2,11,36] for constructing coarse-grid operators in a robust way [15,16,35] and incomplete decomposition based smoothers [28,38]. The high recursivity of incomplete decomposition methods in the smoothing steps would yield a poor parallel efficiency, motivating the search for new multigrid methods. Thus the goal of this study is thus to find robust and parallelizable solution strategies for this partial differential equation. The performances of these strategies will be evaluated on academic and more realistic fluid flow problems. These applications have been performed in the framework of the HORUS computational fluid dynamics code developed by the CFD group in Nantes. Further details on the solution strategy (discretization schemes, pressure-velocity coupling algorithm, accuracy, etc.) can be found in [6].

3. A nonstandard multigrid method

In this section the chosen nonstandard multigrid method is presented for both 2- and 3-dimensional applications.

3.1. Principles

Nonstandard multigrid methods involve a combination of rather local smoothers and robust coarse-grid corrections based on semicoarsened grids, where the semicoarsening means that the coarsening takes place only in one direction.

3.2. An incomplete review of nonstandard multigrid methods

Following the ideas of Hackbusch [11,12] and Brandt [3], Mulder proposed a new technique (Multiple Semicoarsened Grids (MSG)) employing semicoarsening in order to obtain parallel efficiency [19] for CFD applications. Whereas standard coarsening corresponds to the grid sequence (l_x, l_y) with $l_x = l_y$ (see figure 1(a)), figure 1(b)

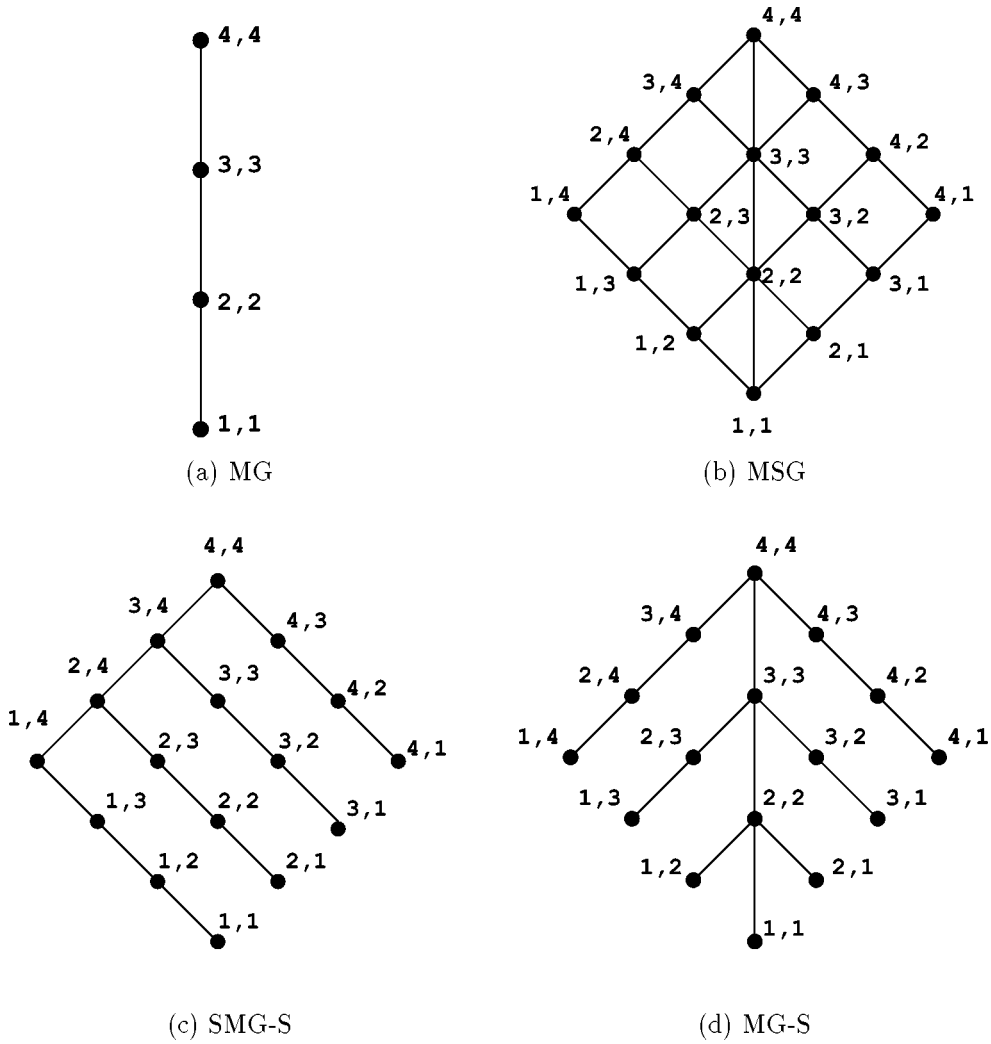

Figure 1. Sequences of grids: (a) for standard multigrid (MG), (b) for Multiple Semicoarsened Grids (MSG), (c) for Semicoarsened MultiGrid as a Smoother (SMG-S), (d) for MultiGrid as a Smoother (MG-S).

presents this nonstandard multigrid hierarchy where the (l_x, l_y) indices correspond to the grid indices respectively in x- and y-directions. Applications to the steady Euler equations of compressible gas dynamics are discussed in [19] for first-order upwind discretization and in [20] for higher-order discretizations. As shown in figure 1(b), coarse-grid information in MSG for the level (l_s, l_s) (say, $l_s < l$, where l is the finest grid level) come from two finer grids simultaneously (levels $(l_s, l_s + 1)$ and $(l_s + 1, l_s)$). This grid structure, therefore, requires the use of weights for combining fine grid information. This requirement may be a serious drawback of MSG leading to difficulties when constructing satisfactory coarse-grid corrections for a large class

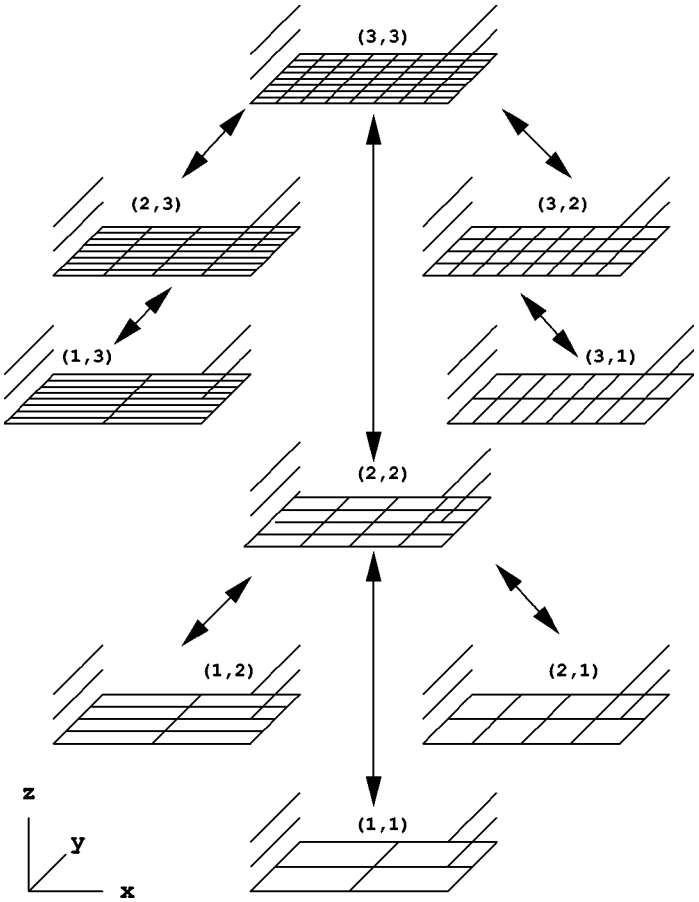

Figure 2. The full 3-dimensional MG-S method with semicoarsening in x- and y-directions and a line smoother in the z-direction.

of problems [21]. An alternative proposed by Washio et al. [33] is the semicoarsened MultiGrid as a Smoother (SMG-S). This technique employs semicoarsening in one direction with semicoarsened multigrid in the second direction as a smoother. In this variant of MSG, coarse-grid information comes from only one grid, yielding a clearer grid structure (see figure 1(c) where (l_s, l_s) is connected only to the finest level $(l_s, l_s + 1)$).

Numerical experiments prove that methods based on strictly semicoarsened grids like MSG or SMG-S are efficient when anisotropies or dominant processes (e.g., convection) are located along one of the axes. Nevertheless, to design a robust solver, singular perturbations not located along an axis must be taken into account. This motivation led Oosterlee to propose the MultiGrid as a Smoother method (MG-S) [22]. Its basis is the standard multigrid method with a semicoarsened multigrid V-cycle in x- and y-directions as a smoother. Figure 1(d) or figure 2 describe the resulting grid sequence. Note that semicoarsened grids are only connected with at most one of the grids of the standard grid sequence.

Why choosing MG-S? A full 3-dimensional method based on semicoarsening with a point smoother would generally need a large number of grids to obtain sufficient robustness. This aspect induces an expensive method on a parallel machine, both in terms of storage and computational work. Thus, MG-S [34] is essentially adopted for its great flexibility, its robustness and its ability to treat 3-dimensional problems. A 3-dimensional nonstandard variant – still of complexity O(N) – is actually deduced from the 2-dimensional one by using MG-S in the x- and y-directions and a z-line smoother in the third one. Thus, coarsening does not take place on the z-direction as depicted in figure 2. Numerical experiments on model problems [34] tend to prove that this choice yields both parallel efficiency and robustness.

3.3. Algorithms

Smoother on the semicoarsened grids. The MG-S method is presented here in more detail. This method uses as a smoother a one-dimensional multigrid method on the semicoarsened grids. One smoothing step consists in smoothing first on the x-semicoarsened grids and then on the y-semicoarsened grids. Only one V-cycle denoted by V_x or V_y with μ_1 and μ_2 pre- and post-smoothing steps is employed. Algorithm 1 presents the V_x multigrid cycle on x-semicoarsened grids $V_x(\mathbf{A}^{l_x,l_y}, \phi^{l_x,l_y}, b^{l_x,l_y}, \mu_1, \mu_2)$. $\mathbf{R}_x$ and $\mathbf{P}_x$ the transfer operators on the x-semicoarsened grids and S the smoother are introduced. The y-counterpart $V_y(\mathbf{A}^{l_x,l_y}, \phi^{l_x,l_y}, b^{l_x,l_y}, \mu_1, \mu_2)$ can be easily deduced from algorithm 1.

Algorithm 1. $V_x(\mathbf{A}^{l_x,l_y}, \phi^{l_x,l_y}, b^{l_x,l_y}, \mu_1, \mu_2)$

(#) Pre-smoothing: $\phi^{l_x,l_y} = S(\mathbf{A}^{l_x,l_y}, \phi^{l_x,l_y}, b^{l_x,l_y}, \mu_1)$

(#) Residual restriction:
$r^{l_x,l_y} = b^{l_x,l_y} - \mathbf{A}^{l_x,l_y}\phi^{l_x,l_y}$
$b^{l_x-1,l_y} = \mathbf{R}_x r^{l_x,l_y}$
$\phi^{l_x-1,l_y} = 0.$

(#) Coarse-grid correction:
$\phi^{l_x-1,l_y} = V_x(\mathbf{A}^{l_x-1,l_y}, \phi^{l_x-1,l_y}, b^{l_x-1,l_y}, \mu_1, \mu_2)$

(#) Prolongation: $\phi^{l_x,l_y} = \phi^{l_x,l_y} + \mathbf{P}_x\phi^{l_x-1,l_y}$

(#) Post-smoothing: $\phi^{l_x,l_y} = S(\mathbf{A}^{l_x,l_y}, \phi^{l_x,l_y}, b^{l_x,l_y}, \mu_2)$

General algorithm. The nonstandard multigrid algorithm named in the following $MG^{(\mu_1,\mu_2)}(\mathbf{A}^{l_x,l_y}, \phi^{l_x,l_y}, b^{l_x,l_y}, \nu_1, \nu_2)$ is presented in algorithm 2.

Algorithm 2. $MG^{(\mu_1,\mu_2)}(\mathbf{A}^{l_x,l_y}, \phi^{l_x,l_y}, b^{l_x,l_y}, \nu_1, \nu_2)$

(#) Pre-smoothing on the x- and y-semicoarsened grids:
For it $= 1, \nu_1$ **do**
$\phi^{l_x,l_y} = V_x(\mathbf{A}^{l_x,l_y}, \phi^{l_x,l_y}, b^{l_x,l_y}, \mu_1, \mu_2)$
End for

(#) Residual restriction:
$r^{l_x,l_y} = b^{l_x,l_y} - \mathbf{A}^{l_x,l_y}\phi^{l_x,l_y}$
$b^{l_x-1,l_y-1} = \mathbf{R}r^{l_x,l_y}$
$\phi^{l_x-1,l_y-1} = 0.$

(#) Coarse-grid correction:
For it $= 1, \gamma$ **do**
$\phi^{l_x-1,l_y-1} = MG^{(\mu_1,\mu_2)}(\mathbf{A}^{l_x-1,l_y-1}, \phi^{l_x-1,l_y-1}, b^{l_x-1,l_y-1}, \nu_1, \nu_2)$
End for

(#) Prolongation:
$\phi^{l_x,l_y} = \phi^{l_x,l_y} + \mathbf{P}\phi^{l_x-1,l_y-1}$

(#) Post-smoothing on the x- and y-semicoarsened grids:
For it $= 1, \nu_2$ **do**
$\phi^{l_x,l_y} = V_x(\mathbf{A}^{l_x,l_y}, \phi^{l_x,l_y}, b^{l_x,l_y}, \mu_1, \mu_2)$
$\phi^{l_x,l_y} = V_y(\mathbf{A}^{l_x,l_y}, \phi^{l_x,l_y}, b^{l_x,l_y}, \mu_1, \mu_2)$
End for

It performs ν_1 and ν_2 pre- and post-smoothing iterations of V_x and V_y cycles. The transfer operators on semicoarsened grids ($\mathbf{R}_x$, $\mathbf{P}_x$, $\mathbf{R}_y$ and $\mathbf{P}_y$) or on coarse grids ($\mathbf{R}$ and $\mathbf{P}$) have to be detailed for the construction of coarse and semicoarsened grid operators by Galerkin approximation. Finally, the smoother S has to be chosen. Further details on MG-S (storage and computational complexity) can be found in [34].

3.4. Galerkin coarse-grid approximation

We now examine the construction of the 2- and 3-dimensional coarse-grid operators defined by the Galerkin coarse-grid approximation [2,11,36]:

$$\mathbf{A}^{l-1,l-1} = \mathbf{R}\mathbf{A}^{l,l}\mathbf{P}. \tag{10}$$

Two-dimensional part. The Galerkin coarse-grid approximation is applied with the following operators $\mathbf{R}_{2D}$ (arithmetic average) and $\mathbf{P}^*_{2D}$ (linear interpolation in a triangle) (see [25] for more details) given in stencil notation (see [36]):

$$[\mathbf{R}_{2D}] = \frac{1}{4}\begin{bmatrix} 1 & 1 \\ 1 & 1 \end{bmatrix}, \qquad [\mathbf{P}^*_{2D}] = \frac{1}{4}\begin{bmatrix} nw & n & 0 & 0 \\ w & 4-nw & \underline{4-n-e} & 0 \\ 0 & 4-w-s & 4-se & e \\ 0 & 0 & s & se \end{bmatrix}. \tag{11}$$

$\mathbf{R}_{2D}$ denotes the restriction operator and $\mathbf{P}^*_{2D}$ stands for the adjoint of the prolongation operator, where the prolongation is defined by the following algebraic rule:

$$\forall k \in \mathcal{G} \quad \left(\mathbf{P}_{2D}\overline{\psi}\right)_k = \sum_{i\in\mathcal{Z}^d} \mathbf{P}^*_{2D}(i, k-2i)\overline{\psi}_i, \tag{12}$$

where i is a multiple index parameter (note that the underlined term in $\mathbf{P}^*_{2D}$ refers to $\mathbf{P}^*(i,0)$, see [36] for more details). After exploitation of symmetry and singularity conditions, $\mathbf{A}^{l-1,l-1}$ is a symmetric singular M-matrix with a five-point structure [15].

Three-dimensional part. The Galerkin coarse grid approximation is generally more tedious for 3-dimensional applications with standard coarsening. As sketched in figure 2, coarsening or semicoarsening is only realized in the x- or y-directions, while the z-direction is left invariant. Thus, following the adopted choice for 2-dimensional applications, a Galerkin coarse-grid approximation is used with the following 3-dimensional transfer operators $\mathbf{R}_{3D}$ and $\mathbf{P}^*_{3D}$, whose projections in the (x–y)-plane are defined in stencil notation by

$$[\mathbf{R}_{3D}]_{xy} = \frac{1}{4}\begin{bmatrix} 1 & \underline{1} \\ 1 & 1 \end{bmatrix}, \qquad \left[\mathbf{P}^*_{3D}\right]_{xy} = \frac{1}{4}\begin{bmatrix} nw & n & 0 & 0 \\ w & 4-nw & \underline{4-n-e} & 0 \\ 0 & 4-w-s & 4-se & e \\ 0 & 0 & s & se \end{bmatrix}. \quad (13)$$

With such restriction and prolongation operators, applying relation (10) inductively on the whole sequence of standard grids leads to a 3-dimensional operator with 21 elements with the following stencil:

$$[\mathbf{A}]^{-1} = \begin{bmatrix} \circ & \star & \\ \star & \star & \star \\ & \star & \circ \end{bmatrix}, \qquad [\mathbf{A}]^{0} = \begin{bmatrix} \circ & \star & \\ \star & \# & \star \\ & \star & \circ \end{bmatrix}, \qquad [\mathbf{A}]^{+1} = \begin{bmatrix} \circ & \star & \\ \star & \star & \star \\ & \star & \circ \end{bmatrix}. \quad (14)$$

This stencil explosion is already a drawback. Moreover, this construction numerically leads to off-diagonal elements of different signs (elements marked by $\circ$ are found to be positive for diffusion-dominated problems, whereas $\star$ elements are negative). This feature leads to a divergence of the smoothing process on coarse grids, because the M-matrix property is lost. This behaviour will also affect the semicoarsened grid operators. A cure is proposed here. From the 3-dimensional operator $\mathbf{A}$, a 2-dimensional discrete fine-grid operator $\widetilde{\mathbf{A}}$ of generic term $\widetilde{a}_{nb}$ is defined:

$$\left[\widetilde{\mathbf{A}}\right] = \begin{bmatrix} a_7 + a_{16} + a_{25} & a_8 + a_{17} + a_{26} & a_9 + a_{18} + a_{27} \\ a_4 + a_{13} + a_{22} & a_5 + a_{14} + a_{23} & a_6 + a_{15} + a_{24} \\ a_1 + a_{10} + a_{19} & a_2 + a_{11} + a_{20} & a_3 + a_{12} + a_{21} \end{bmatrix}. \quad (15)$$

For our study, the fine-grid operator $\widetilde{\mathbf{A}}$ structure corresponds to

$$\left[\widetilde{\mathbf{A}}\right] = \begin{bmatrix} 0 & \widetilde{a}_8 & 0 \\ \widetilde{a}_4 & \widetilde{a}_5 & \widetilde{a}_6 \\ 0 & \widetilde{a}_2 & 0 \end{bmatrix} = \begin{bmatrix} 0 & a_8 & 0 \\ a_4 & a_5 + a_{14} + a_{23} & a_6 \\ 0 & a_2 & 0 \end{bmatrix}. \quad (16)$$

A five-point stencil is thus obtained, fulfilling the relation

$$\sum_i \widetilde{a}_i = 0. \quad (17)$$

$\widetilde{\mathbf{A}}$ is a symmetric singular 2-dimensional operator. This construction allows the recovery of the previously presented 2-dimensional operator properties. The Galerkin coarse-grid approximation is, therefore, applied with transfer operators (11) and leads to a five-point stencil on each coarse grid:

$$\left[\overline{\mathbf{A}}\right]^0 = \begin{bmatrix} 0 & \overline{\widetilde{a}_8} & 0 \\ \overline{\widetilde{a}_4} & \star & \overline{\widetilde{a}_6} \\ 0 & \overline{\widetilde{a}_2} & 0 \end{bmatrix}. \tag{18}$$

At this stage and except for the central element $\star$, the off-diagonal elements of the true coarse-grid operator $\overline{\mathbf{A}}$ are built only in the plane $iz = 0$. The z-direction coefficients and the central element $\overline{a_5}$ remain to be built. An isotropic approximation is proposed for the coefficients involved in the z-direction, i.e.

$$\overline{a_{14}}_{i,j,k} = \frac{1}{4}(a_{142i-1,2j-1,k} + a_{142i,2j-1,k} + a_{142i-1,2j,k} + a_{142i,2j,k}), \tag{19}$$

$$\overline{a_{23}}_{i,j,k} = \frac{1}{4}(a_{232i-1,2j-1,k} + a_{232i,2j-1,k} + a_{232i-1,2j,k} + a_{232i,2j,k}). \tag{20}$$

Finally, the central element $\overline{a_5}$ is built by fulfilling the singularity condition

$$\overline{a_5}_{i,j,k} = -\sum_{nb} \overline{a_{nb}}_{i,j,k}. \tag{21}$$

This construction allows optimal sparsity and keeps the symmetry condition on each coarse grid.

3.5. *Galerkin semicoarsened grid approximation*

We detail here the construction of the 2- and 3-dimensional x-semicoarsened and y-semicoarsened grid operators defined by

$$\mathbf{A}^{l_x-1,l_y} = \mathbf{R}_x \mathbf{A}^{lx,ly} \mathbf{P}_x, \tag{22}$$

$$\mathbf{A}^{l_x,l_y-1} = \mathbf{R}_y \mathbf{A}^{lx,ly} \mathbf{P}_y. \tag{23}$$

Two-dimensional part. The following transfer operators have been chosen in the x- and y-directions, respectively:

$$[\mathbf{R}_x] = \frac{1}{2}\begin{bmatrix} 1 & \underline{1} \end{bmatrix}, \qquad \left[\mathbf{P}_x^*\right] = \frac{1}{4}\begin{bmatrix} w & 4-w & \underline{4-e} & e \end{bmatrix} \tag{24}$$

and

$$[\mathbf{R}_y] = \frac{1}{2}\begin{bmatrix} 1 \\ \underline{1} \end{bmatrix}, \qquad \left[\mathbf{P}_y^*\right] = \frac{1}{4}\begin{bmatrix} n \\ 4-n \\ \underline{4-s} \\ s \end{bmatrix}. \tag{25}$$

The coefficients of the x- or y-semicoarsened grid operators are detailed in [32]. Note that these operators now have a nine-point structure.

Three-dimensional part. By construction, each coarse grid operator has a 7 point structure. By analogy, the following transfer operators are adopted (for instance, in the x-direction):

$$[\mathbf{R}_x] = \frac{1}{2}\begin{bmatrix} 1 & \underline{1} \end{bmatrix}, \qquad \begin{bmatrix} \mathbf{P}_x^* \end{bmatrix} = \frac{1}{4}\begin{bmatrix} w & 4-w & \underline{4-e} & e \end{bmatrix}. \tag{26}$$

Application of Galerkin approximation (22) or (23) leads to a compact 15 point structure for x- and for y-semicoarsening [32]. Note that the M-matrix property is fulfilled on each semicoarsened grid.

3.6. Smoother

Two-dimensional part. As pointed out in algorithm 1, each semicoarsened multigrid method V_x or V_y needs a smoother called S. For 2-dimensional applications, a point smoother is sufficient in the framework of any semicoarsening technique. Therefore, a four-color point Gauss–Seidel smoother allowing the vectorization or parallelization of the smoothing procedure for nine-point stencil is used with a relaxation parameter equal to 0.9.

Three-dimensional part. According to the generalization of MG-S evoked in section 3.2, here S denotes a z-line Gauss–Seidel relaxation with a zebra ordering. A relaxation parameter equal to 0.9 is chosen.

3.7. Flexible coarsening

As soon as isotropic or nearly isotropic problems are treated on semicoarsened grids, coarsening is no longer useful. This led Washio and Oosterlee to propose a more flexible variant of MG-S [34]. This variant has been adopted in this work for purely diffusive problems like (1). The parameter involved in the condition to stop or not the semicoarsening (δ_1 in [34]) is here equal to 0.9. See [34] for more details.

3.8. Implementation details

The MG-S method with flexible multiple semicoarsening leads to a rather complex recursive algorithm (in fact, a standard multigrid method with a lower dimensional alternating semicoarsened multigrid smoother). Therefore, to cope with such difficulties, Fortran 90 has been adopted as programming language. Fortran 90 allows recursion, hence, the multigrid schedules (algorithms 1, 2) can be programmed in a straightforward way for any cycling strategy (V-, F- and W-cycle). Moreover, the use of derived type structure has been exploited in the current implementation. A structure contains all relevant information related to a grid level (l_x, l_y) of the grid sequence (dimensions in each direction, discretization coefficients, solution, right-hand

side, etc.). The data structure consisting of arrays of this structure is accessed via the structure corresponding to that level. Both features (derived type structure and recursion) combined with dynamic memory allocation are valuable tools for designing a safe implementation.

4. Numerical experiments

In this section, the nonstandard multigrid method with flexible semicoarsening is applied to the numerical solution of the pressure problem (equations (1)–(3)). The goal of these experiments is to present the performances of the developed multigrid method evaluated both as a solver as well as a preconditioner for Krylov subspace methods (BiCGSTAB and GMRES [27]) as well as to test the resulting robustness. The numerical experiments were carried out in double precision arithmetic on a Silicon Graphics workstation equipped with one 190 MHz R10000 processor.

4.1. Two-dimensional part

Two fluid flow simulations are considered: The flow in a regular lid-driven cavity at $Re = 1000$ and the turbulent flow around a commercial airfoil (AS240-B) at high incidence (19°, $Re = 2 \cdot 10^6$). F-cycles are used here with one global pre- and post-smoothing iteration ($\nu_1 = \nu_2 = 1$) and as a smoother the multigrid method on the semicoarsened grid with one pre- and post-smoothing iteration ($\mu_1 = \mu_2 = 1$) leading to $F^{(1,1)}(1,1)$-cycle. A reduction factor corresponding to *nbord* orders of magnitude is imposed to compare the efficiency of the different methods:

$$\frac{\|r^{(n)}\|_2}{\|r^{(0)}\|_2} \leqslant 10^{-nbord}, \tag{27}$$

where $\|r^{(n)}\|_2$ denotes the l_2-norm of the linear residual at iteration n ($r^{(n)} = b - \mathbf{A}\phi^n$). For each test-case, *nbord* will be explicitly mentioned. As pointed out in equation (1), the pressure linear system coefficients C_{nn} depend on the nonlinear iteration. Nevertheless, reliable information can be obtained by analysis of the linear system at one nonlinear iteration during the current nonlinear process. Thus, the adopted approach consists in storing the pressure linear system and in studying the performance of the multigrid either as a solver or as a preconditioner.

Flow in a regular lid-driven cavity. This very popular fluid flow problem [9] serves as a first illustration. It includes many physical features (recirculation, boundary layers, singularities) explaining its choice. The Reynolds number is set to 1000. An orthogonal stretched grid in both directions has been used. As proposed in [34], grid generation was handled by a Gauss–Lobatto–Legendre (GLL) rule to make further comparisons

Table 1
Regular lid-driven cavity ($Re = 1000$): number of cycles (*Nbcy*) or number of Krylov subspace iterations (*Nit*) for multigrid used as a solver (Solv.) or as a preconditioner (Prec.) ($F^{(1,1)}(1,1)$-cycle) on several grid sizes.

Grid	64×64	128×128	256×256
Solv. (*Nbcy*)	4	4	4
Prec. (BiCGSTAB) (*Nit*)	2	2	2
Prec. (GMRES(20)) (*Nit*)	4	4	4
Coarsest x-semicoarsened grids (128^2)	full x-semicoarsening		
Coarsest y-semicoarsened grids (128^2)	(6,4) (5,3) (4,3) (3,2)		

easier. The inner grid point coordinates on a $(n_x + 2) \times (n_y + 2)$ node-centered grid are, thus, defined by

$$x(k) = \sqrt{\frac{n_x(n_x+2)}{(n_x+1/2)(n_x+3/2)}} \cos\left(k\frac{\pi}{n_x+1}\right), \quad k \in \{1,\ldots,n_x\}, \tag{28}$$

$$y(k) = \sqrt{\frac{n_y(n_y+2)}{(n_y+1/2)(n_y+3/2)}} \cos\left(k\frac{\pi}{n_y+1}\right), \quad k \in \{1,\ldots,n_y\}. \tag{29}$$

As an indication of the stretching, respectively 5 and 11 points are located in $[0.99, 1]$ on the cell-centered 128×128 and 256×256 meshes. The detected nonstandard multigrid sequence for this 128×128 grid is presented in table 1. An interesting feature is to note that this grid sequence is not symmetric, although relations (28) and (29) (with $n_x = n_y$) induce a symmetric repartition of grid points in the x- and y-directions. This aspect highlights the anisotropic nature of the $C_{nn}R_{\text{eff}}/(1+e_1C_{nn})$ coefficients in the pressure operator. Table 1 collects the number of cycles ($Nbcy$) or the number of BiCGSTAB or GMRES(m) ($m = 20$) iterations (*Nit*) required to fulfill the convergence criterion (27) with *nbord* $= 6$ on various meshes. Grid-independent convergence rates are found for this first illustration. Note that both Krylov subspace methods require the same number of preconditioning steps, since the preconditioning cost per iteration in BiCGSTAB is twice as high as the one of GMRES(m).

Flow around an airfoil at high incidence. The second application deals with the steady simulation of turbulent viscous fluid flow around a commercial airfoil AS240-B at fixed high incidence (19°), with a Reynolds number set to $2 \cdot 10^6$. Turbulence modeling is handled by a $K-\omega$ two-equation model proposed by Wilcox [37]. The goal of such a simulation consists in predicting as accurately as possible the stalling behavior of this airfoil – corresponding to a maximum drag and peak-suction incidence – for enhancing the airfoil geometry during the phases of take-off and landing; see the discussion of Guilmineau et al. [10] for more details. Due to a high mesh resolution down to the wall, the resulting pressure linear system is strongly ill-conditioned. Thus, the goal of this study is to test the robustness on a given severely stretched O-type mesh.

Table 2
AS240-airfoil at high incidence (19°, $Re = 2 \cdot 10^6$): number of cycles (*Nbcy*) or number of Krylov subspace iterations (*Nit*) for multigrid used as a solver (Solv.) or as a preconditioner (Prec.) ($F^{(1,1)}(1,1)$-cycle) on the 128×128 mesh.

Grid	128×128
Solv. (*Nbcy*)	4
Prec. (BiCGSTAB) (*Nit*)	3
Prec. (GMRES(20)) (*Nit*)	4
Coarsest x-semicoarsened grids	no x-semicoarsening
Coarsest y-semicoarsened grids	(6,2) (5,1) (4,1) (3,1) (2,1)

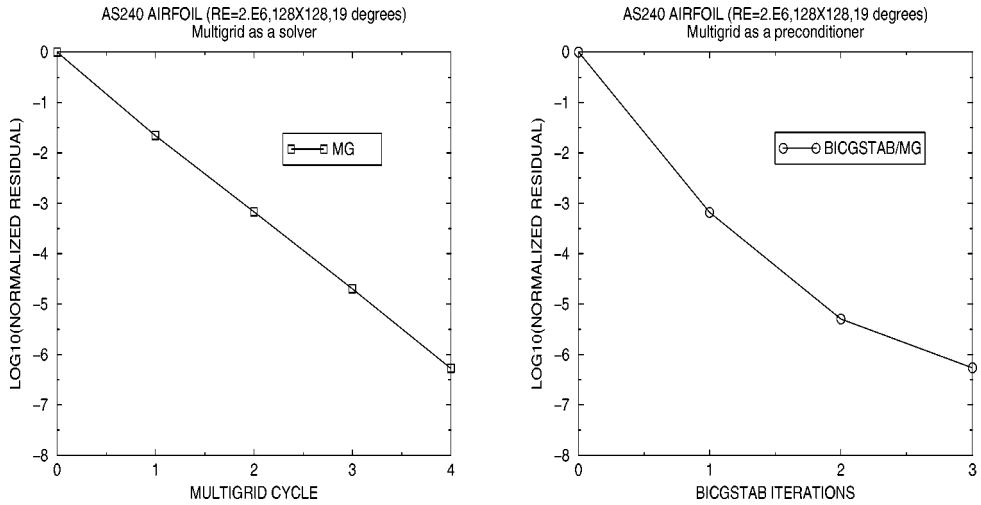

Figure 3. AS240-airfoil at high incidence (19°, $Re = 2 \cdot 10^6$, 128×128): convergence curves for multigrid used as a solver (left) and multigrid used as a preconditioner (BiCGSTAB) (right) ($F^{(1,1)}(1,1)$-cycle.)

Table 2 details the detected grid sequence. Note that coarsening takes place only in the radial direction, where high stretching is used to be able to capture the boundary layer and the wake region. Table 2 collects the results for the nonstandard multigrid method as a solver or as a preconditioner to fulfill relation (27) with *nbord* = 6. The convergence curves for the multigrid used as a solver or as a preconditioner are presented in figure 3.

The corresponding average reduction factor defined by

$$\overline{\kappa} = \left(\frac{\|r^{(\nu)}\|_2}{\|r^{(0)}\|_2} \right)^{1/\nu}, \tag{30}$$

where ν denotes the number of multigrid cycles to fulfill the stopping criterion, is equal to 0.03. This result is very satisfactory for such an anisotropic problem. To understand the robustness of the multigrid preconditioning approach, the eigenvalue spectrum of the Richardson iteration matrix $\mathbf{I} - \mathbf{AM}^{-1}$, where $\mathbf{M}$ denotes the preconditioner – here the iteration matrix of the multigrid method [11] – is determined, a technique already

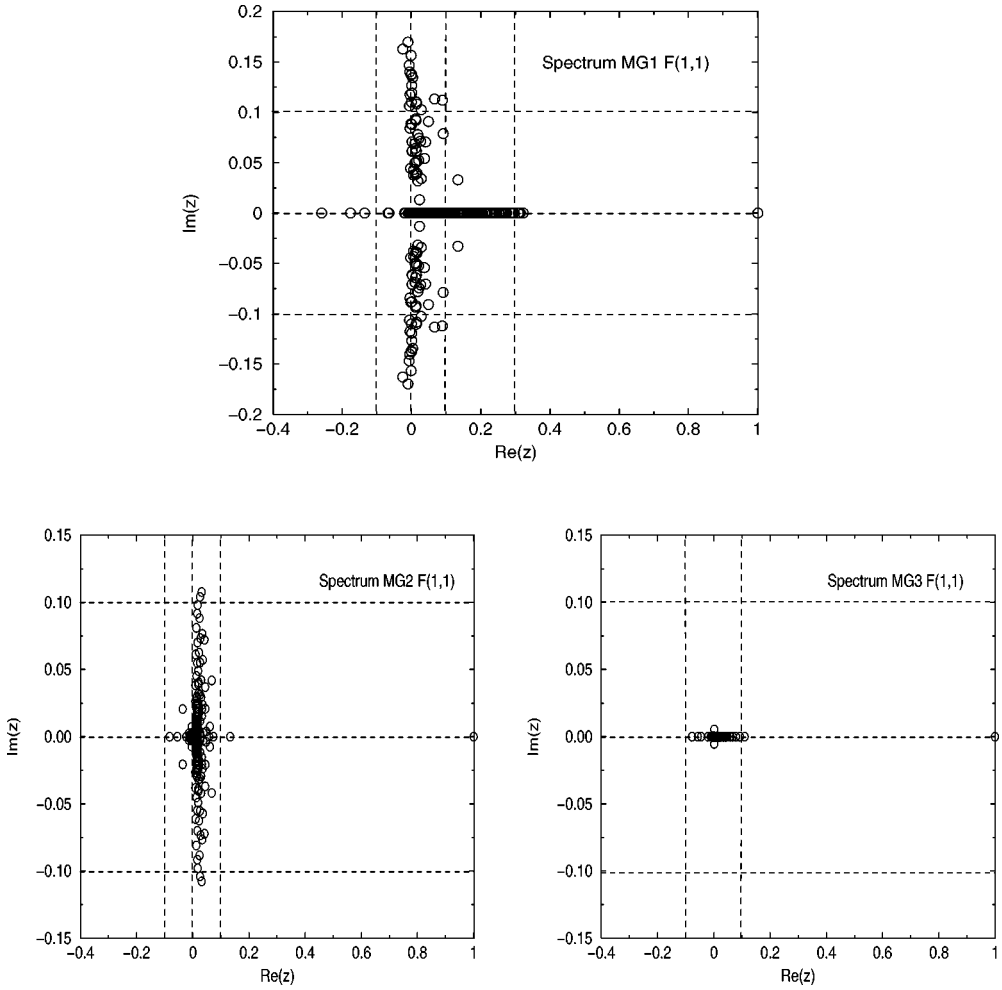

Figure 4. AS240-airfoil at high incidence (19°, $Re = 100$, 32×32): eigenvalue spectrum of the multigrid iteration matrix with methods MG1, MG2 and MG3.

proposed in [23]. Due to memory limitation requirements ($\mathbf{I} - \mathbf{AM}^{-1}$ is a dense matrix of size $n_x \times n_y$, if the domain is discretized on a $n_x \times n_y$ grid), the elliptic pressure problem is solved on a rather coarse mesh of dimensions 32×32 at $Re = 100$. Three multigrid methods with common properties (cell-centered coarsening, Galerkin approximation with matrix-independent transfer operators) have been compared:

- MG1: a standard multigrid method with a point smoother (four-color point Gauss–Seidel);
- MG2: a standard multigrid method with a line smoother (zebra-line Gauss–Seidel);
- MG3: the MG-S nonstandard method.

The three spectra are represented in figure 4. Corresponding average reduction factors are $\overline{\kappa}_{\mathrm{MG1}} = 0.315$, $\overline{\kappa}_{\mathrm{MG2}} = 0.1337$ and $\overline{\kappa}_{\mathrm{MG3}} = 0.1096$. Due to the singularity of operator **A**, all three Richardson operators have a unique unit eigenvalue. As can be seen, most eigenvalues are clustered around 0 for MG2 and MG3, in contrast to MG1. The MG1 spectrum illustrates a well-known rule: a point smoother is clearly unsuitable for this anisotropic problem. In the standard multigrid, a line smoother is, therefore, mandatory, involving better smoothing properties. Analysis of the MG3 spectrum reveals that the spectral radius is very close to the average reduction factor. This solver needs a local (and therefore well-parallelizable) smoother in contrast to line smoothers, where the parallelization strategy is not so obvious (see [18,33]).

4.2. Three-dimensional part

Section 4.1 has shown the robustness of the nonstandard multigrid method for 2-dimensional applications (see also [32] for experiments on model problems). Since the basis of the 3-dimensional solver is a 2-dimensional nonstandard multigrid method, this previous part was of relevant importance. The goal of this section is to demonstrate the ability of the nonstandard multigrid to solve 3-dimensional model and realistic problems.

4.2.1. General anisotropic diffusion model problem

The first application is a well-known test for robustness: the general anisotropic diffusion equation [29] here with Neumann-type boundary conditions on all sides of the computational domain Ω:

$$-\varepsilon_1 \frac{\partial^2 \phi}{\partial x^2} - \varepsilon_2 \frac{\partial^2 \phi}{\partial y^2} - \varepsilon_3 \frac{\partial^2 \phi}{\partial z^2} = f \quad \text{on } \Omega = [0,1] \times [0,1] \times [0,1], \tag{31}$$

$$\left.\frac{\partial \phi}{\partial n}\right|_{x=0,y,z} = \left.\frac{\partial \phi}{\partial n}\right|_{x,y=0,z} = \left.\frac{\partial \phi}{\partial n}\right|_{x,y,z=0} = 0, \tag{32}$$

$$\left.\frac{\partial \phi}{\partial n}\right|_{x=1,y,z} = \left.\frac{\partial \phi}{\partial n}\right|_{x,y=1,z} = \left.\frac{\partial \phi}{\partial n}\right|_{x,y,z=1} = 0. \tag{33}$$

A robust solver must be able to solve efficiently this problem – denoted (P3D) in the following – for all parameter sets. Moreover, as advocated in [34], the ε_i parameters ($i = 1, 3$) are permuted along the three directions in order to investigate the effect of a rotation of axes on the robustness. Table 3 presents the results for MG-S as a solver or as a preconditioner on various meshes and for different parameter sets. Eight orders of magnitude (*nbord* $= 8$) is the stopping criterion. Figure 5 presents the grid sequences for the different parameter sets on the finest considered grid, 64^3. The isotropic problem (case I) or dominant direction problems (case IIa or case IIb) are correctly solved: grid-independent convergence rates are found. Note that the isotropic problem (case I) induces a natural grid sequence (the standard one) and that the grid sequences of cases IIb and IIIa are symmetric. Both these features contrast

Table 3
Number of cycles for multigrid used as a solver (Solv.) and number of BiCGSTAB iterations for multigrid used as a preconditioner (Prec.) for solving anisotropic diffusion problem (P3D) ($F^{(1,1)}(1,1)$-cycle) on several grid sizes. Cases in bold correspond to no semicoarsening.

$$-\varepsilon_1\frac{\partial^2\phi}{\partial x^2}-\varepsilon_2\frac{\partial^2\phi}{\partial y^2}-\varepsilon_3\frac{\partial^2\phi}{\partial z^2}=f$$

Case	ε_1	ε_2	ε_3	Mode	16^3	32^3	64^3	Mode	16^3	32^3	64^3
I	**1**	**1**	**1**	Solv.	8	8	8	Prec.	3	4	4
IIa	**1**	**1**	**100**	Solv.	6	6	6	Prec.	3	3	3
IIb	1	100	1	Solv.	6	6	6	Prec.	3	3	3
IIIa	100	1	100	Solv.	8	8	8	Prec.	4	4	4
IIIb	**100**	**100**	**1**	Solv.	8	8	8	Prec.	4	4	4
IVa	1	100	0.01	Solv.	10	10	10	Prec.	4	5	5
IVb	100	0.01	1	Solv.	10	10	10	Prec.	4	5	5

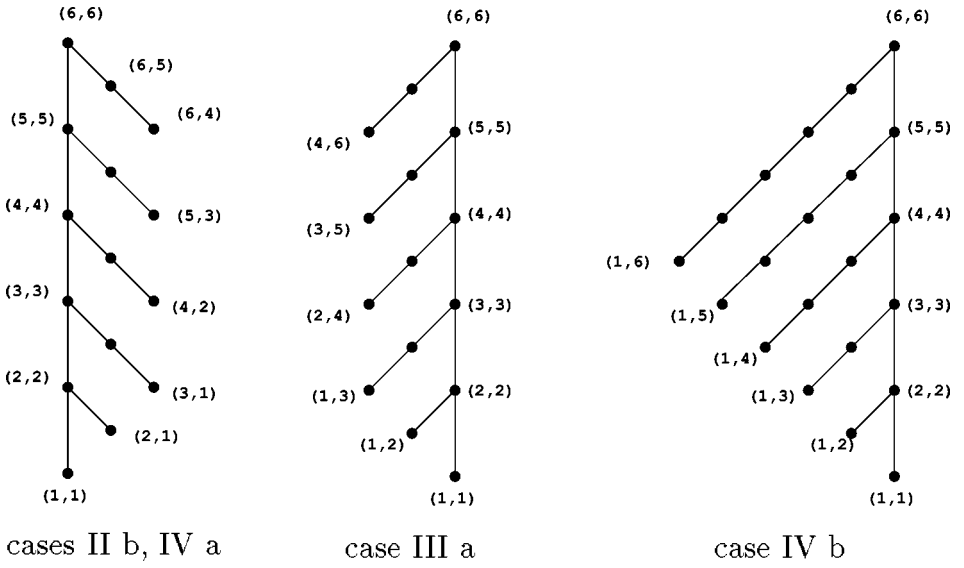

Figure 5. MG-S detected grid sequences on the $64\times64\times64$ grid for solving anisotropic diffusion model problem (P3D). Other cases correspond to no semicoarsening.

with the results of Washio and Oosterlee, where unusual coarsening was sometimes observed; that was attributed to the adopted lumping strategy (see [34] for more details). Cases IIIa and IIIb are well-known pathological cases in the standard multigrid [1], where a plane smoother is really mandatory. These problems are also satisfactorily handled, yielding grid-independent convergence rates. The flexible coarsening strategy works well, leading to impressive storage benefits with respect to full 3-dimensional semicoarsening. Note that, although the 3-dimensional variant of MG-S is not invariant with respect to rotation of axes, no sensitivity in the results is found for this application.

Table 4
Regular lid-driven cavity ($Re = 100$): number of cycles (*Nbcy*) or number of Krylov subspace iterations (*Nit*) for multigrid used as a solver (Solv.) or as a preconditioner (Prec.) ($F^{(1,1)}(1,1)$-cycle) on several grid sizes.

Grid	16^3	32^3	64^3
Solv. (*Nbcy*)	5	6	5
Prec. (BiCGSTAB) (*Nit*)	3	3	3
Coarsest x-semicoarsened grids (64^3)	full x-semicoarsening		
Coarsest y-semicoarsened grids (64^3)	(6,4)	(5,4)	(4,3)

Table 5
L-shaped lid-driven cavity ($Re = 100$): number of cycles (*Nbcy*) or number of Krylov subspace iterations (*Nit*) for multigrid used as a solver (Solv.) or as a preconditioner (Prec.) ($F^{(1,1)}(1,1)$-cycle) on several grid sizes.

Grid	16^3	32^3
Solv. (*Nbcy*)	9	9
Prec. (BiCGSTAB) (*Nit*)	4	4
Coarsest x-semicoarsened grids (32^3)	no x-semicoarsening	
Coarsest y-semicoarsened grids (32^3)	(5,4) (4,3)	(3,2)

4.2.2. Flow in regular and L-shaped lid-driven cavities

The second illustration is the generalization of the first 2-dimensional example: the simulation of the fluid flow in lid-driven cavities. Two geometric configurations are treated. First, a regular lid-driven cavity is adopted, where the grid generation is handled by the same tensor product technique (GLL). Thus, stretching occurs in all three directions. Secondly, an L-shaped lid-driven cavity has also been tested. This benchmark test-case [24] offers a good example to examine the influence of curvature upon robustness. Stretched curvilinear grids are used in each (x–y)-plane, uniform mesh size is used in the third one.

Tables 4 and 5 detail the two detected grid sequences. Once again note that the grid sequence related to the regular lid-driven cavity is not symmetric. The same explanation as before is available. The L-shaped cavity grid sequence illustrates the potential savings of the flexible coarsening condition. Tables 4 and 5 collect the results of MG-S as a solver and as a preconditioner for both geometries. Ten orders of magnitude ($nbord = 10$) is the stopping criterion. Note that for the L-shaped lid-driven cavity test-case, MG-S with a $F^{(1,1)}(1,1)$-cycle induces an average reduction factor close to 0.078. These results reveal the real robustness of MG-S. Robustness is not impaired either by grid stretching or curvilinearity. Again grid-independent convergence rates are found for these two academic examples.

4.2.3. Flow around the HSVA tanker

The last application concerns the simulation of the turbulent flow around a complex 3-dimensional geometry (a tanker hull) at high Reynolds number ($5 \cdot 10^6$) on a

Table 6
HSVA tanker ($Re = 5 \cdot 10^6$): number of cycles (*Nbcy*) or number of Krylov subspace iterations (*Nit*) for multigrid used as a solver (Solv.) or as a preconditioner (Prec.) ($F^{(1,1)}(1,1)$-cycle) on the $96 \times 48 \times 32$ mesh.

Grid	$96 \times 48 \times 32$
Solv. (*Nbcy*)	10
Prec. (BiCGSTAB) (*Nit*)	4
Coarsest x-semicoarsened grids	full x-semicoarsening
Coarsest y-semicoarsened grids	(5,3) (4,2) (3,1) (2,1)

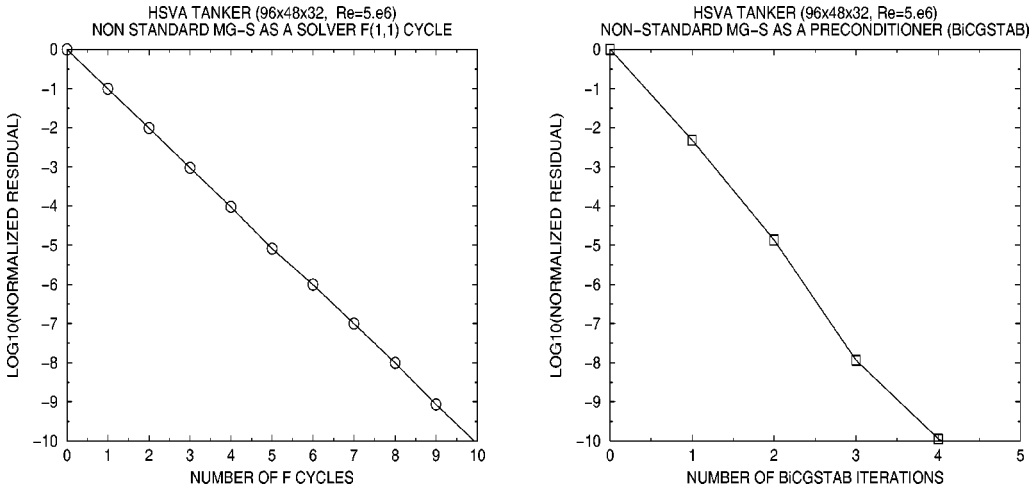

Figure 6. HSVA tanker ($Re = 5 \cdot 10^6$, $96 \times 48 \times 32$): convergence curves for multigrid used as a solver (left) and multigrid used as a preconditioner (BiCGSTAB) (right) ($F^{(1,1)}(1,1)$-cycle.)

$96 \times 48 \times 32$ mesh with Baldwin–Lomax as turbulence model. Table 6 and figure 6 collect the results and the convergence curves. Five grid levels are used. To test the robustness, the stopping criterion corresponds to 10 orders of magnitude (*nbord* $= 10$). Here the goal is to analyze on a given mesh the characteristics of MG-S. See [26] for more details about the physics of the flow and [25] for a similar detailed study with standard multigrid methods.

The complexities of both the geometry and the flow induce great difficulties for linear pressure solvers. As can be analyzed, the nonstandard multigrid solver handles this linear system efficiently, yielding an average reduction factor close to 0.1. This value is quite close to the average reduction factors obtained by standard multigrid methods with incomplete decomposition smoothers [25]. This feature seems very attractive, because robustness in MG-S does not inhibit parallel efficiency. This last example illustrates quite well the attractivity of MG-S. Furthermore, note that the Krylov acceleration is again successful and leads to a reliable procedure.

5. Conclusion

A linear multigrid method has been presented that solves 2- or 3-dimensional linear elliptic equations with possibly highly variable coefficients. This multigrid method can be interpreted as a variant of the multigrid method with flexible multiple semicoarsening proposed by Washio and Oosterlee [34]. The main novelty of this variant is the use of the Galerkin method in a *cell-centered formulation* with *matrix-independent* transfer operators. Note that the proposed solution method is expected to lead to a well-parallelizable solution method, since fixed smoothers, fixed transfer operators are used. A grid partitioning can be suggested [18], requiring, therefore, a sequential process of grids. An agglomeration strategy is needed to yield a full parallel efficiency.

Numerical experiments on 2- and 3-dimensional fluid flow problems tend to confirm Washio's and Oosterlee's experience obtained on model problems (both diffusion and convection dominated convection–diffusion problems). This nonstandard multigrid method is both efficient as a solver and as a preconditioner for Krylov subspace methods (BiCGSTAB or GMRES(m)). The latter option seems very promising and represents a noticeable step toward robust and parallel efficient preconditioners for 3-dimensional elliptic problems.

Combining multigrid with flexible semicoarsening may provide in the near future a promising solution method. The approach presented here is expected to be easy to generalize both to nonlinear problems and to systems of equations coming from finite difference or finite volume discretizations. For systems of equations, a local collective smoother would be sufficient, whereas nonlinear problems could be handled with the Full Approximation Scheme (FAS) [2]. Moreover, the robustness of MG-S motivates the design of a concurrent space and time multigrid method for parabolic partial differential equations [13] (i.e., for such 2-dimensional applications, here the time variable would play the role of the third direction (z) in the 3-dimensional variant of MG-S). In view of these developments, we anticipate that MG-S will become an attractive option for the solution of nonlinear time-dependent systems.

References

[1] A. Behie and P. Forsyth, Multigrid solution of three-dimensional problems with discontinous coefficients, Appl. Math. Comput. 13 (1983) 229–240.
[2] A. Brandt, Guide to multigrid development, in: *Proceedings: Multigrid Methods*, eds. W. Hackbusch and U. Trottenberg, Köln-Porz (Springer, Berlin, 1982) pp. 220–312.
[3] A. Brandt, Multi-level adaptive solutions to boundary-value problems, Math. Comp. 31 (1977) 333–390.
[4] A. Brandt, Barriers to achieving Textbook Multigrid Efficiency (TME) in CFD, Icase Interim Report No. 32 (1998).
[5] J.E. Dendy, Black box multigrid, J. Comput. Phys. 48 (1982) 366–386.
[6] G.B. Deng, J. Piquet, P. Queutey and M. Visonneau, Navier–Stokes equations for incompressible flows: Finite-difference and finite-volume methods, in: *Handbook of Computational Fluid Mechanics*, ed. R. Peyret (Academic Press, New York, 1996) pp. 25–97.

[7] P.M de Zeeuw, Matrix-dependent prolongations and restrictions in a blackbox multigrid solver, J. Comput. Appl. Math. 33 (1990) 1–27.
[8] J. Francescatto and A. Dervieux, Semi-coarsening for agglomeration multigrid: Application to turbulent flows, Internat. J. Numer. Methods Fluids 26 (1998) 927–957.
[9] U. Ghia, K.N. Ghia and C. Shin, High Re solutions for incompressible flow using the Navier–Stokes equations and a multigrid method, J. Comput. Phys. 48 (1982) 387–411.
[10] E. Guilmineau, J. Piquet and P. Queutey, Two-dimensional turbulent viscous flows past airfoils at fixed incidence, Comput. & Fluids 26 (1997) 135–162.
[11] W. Hackbusch, *Multigrid Methods and Applications* (Springer, Berlin, 1985).
[12] W. Hackbusch, The frequency domain decomposition multigrid method, Part I: Application to anisotropic equations, Numer. Math. 56 (1989) 229–245.
[13] G. Horton and S. Vandewalle, A space-time multigrid method for parabolic pdes, SIAM J. Sci. Comput. 16(4) (1995) 848–864.
[14] R. Kettler and P. Wesseling, Aspects of multigrid methods for problems in three dimensions, Appl. Math. Comput. 19 (1986) 159–168.
[15] M. Khalil, Analysis of linear multigrid methods for elliptic differential equations with discontinous and anisotropic coefficients, Ph.D. thesis, Department of Technical Mathematics and Informatics, University of Technology, Delft (1989).
[16] M. Khalil and P. Wesseling, Vertex-centered and cell-centered multigrid for interface problems, J. Comput. Phys. 98 (1992) 1–10.
[17] D.J. Mavripilis, Multigrid strategies for viscous flow solvers on anisotropic unstructured meshes, Icase Report 98-6 (1998).
[18] O.A. McBryan, P. Frederickson, J. Linden, A. Schüller, K. Solchenbach, K. Stüben, C. Thole and U. Trottenberg, Multigrid methods on parallel computers – a survey of recent developments, Impact. Comput. Sci. Engrg. 3 (1991) 1–75.
[19] W.A. Mulder, A new multigrid approach to convection problems, J. Comput. Phys. 83 (1989) 303–323.
[20] W.A. Mulder, A high-resolution Euler solver based on multigrid, semicoarsening and defect correction, J. Comput. Phys. 100 (1992) 91–104.
[21] N.H. Naik and J. van Rosendale, The improved robustness of multigrid elliptic solvers based on multiple semicoarsened grids, SIAM J. Numer. Anal. 30 (1993) 215–229.
[22] C.W. Oosterlee, The convergence of parallel multiblock multigrid methods, Appl. Numer. Math. 19 (1995) 115–128.
[23] C.W. Oosterlee and T. Washio, An evaluation of parallel multigrid as a solver and a preconditioner for singular perturbed problems, SIAM J. Sci. Comput. 19(1) (1998) 87–110.
[24] C.W. Oosterlee, P. Wesseling, A. Segal and E. Brakkee, Benchmark solutions for the incompressible Navier–Stokes equations in general coordinates on staggered grids, Internat. J. Numer. Methods Fluids 17 (1993) 301–321.
[25] J. Piquet and X. Vasseur, Multigrid preconditioned Krylov subspace methods for the three-dimensional numerical solution of the incompressible Navier–Stokes equations, Numer. Algorithms 17 (1998) 1–32.
[26] J. Piquet and M. Visonneau, Computation of the flow past shiplike hulls, Comput. & Fluids 19(2) (1991) 183–215.
[27] Y. Saad and M. Schultz, GMRES: A generalized minimal residual algorithm for solving nonsymmetric linear systems, SIAM J. Sci. Statist. Comput. 7 (1986) 856–869.
[28] H. Stone, Iterative solution of implicit approximations of multidimensional partial differential equations, SIAM J. Numer. Anal. 5 (1968) 530–558.
[29] C.A. Thole and U. Trottenberg, Basic smoothing procedures for the multigrid treatment of elliptic 3D-operators, Appl. Math. Comput. 19 (1986) 333–345.

[30] H.A. Van Der Vorst, BiCGSTAB: a fast and smoothly converging variant of BiCG for the solution of nonsymmetric linear systems, SIAM J. Sci. Statist. Comput. 13 (1992) 631–644.
[31] R.S. Varga, *Matrix Iterative Analysis* (Prentice-Hall, Englewood Cliffs, NJ, 1962)
[32] X. Vasseur, Etude numérique de techniques d'accélération de convergence lors de la résolution des équations de Navier–Stokes, Ph.D. thesis, Université de Nantes (1998).
[33] T. Washio and C.W. Oosterlee, Experiences with robust parallel multilevel preconditioners for BiCGSTAB, GMD Arbeitspapier 949, Gesellschaft für Mathematik und Datenverarbeitung, Sankt-Augustin, Germany (1995).
[34] T. Washio and C.W. Oosterlee, Flexible multiple semicoarsening for three-dimensional singularly perturbed problems, SIAM J. Sci. Comput. 19(5) (1998) 1646–1666.
[35] P. Wesseling, Cell-centered multigrid for interface problems, J. Comput. Phys. 79 (1988) 85–91.
[36] P. Wesseling, *An Introduction to Multigrid Methods* (Wiley, Chichester, 1992).
[37] D.C. Wilcox, *Turbulence Modeling for CFD*, DCW Industries (Griffin, London, 1993).
[38] G. Wittum, On the robustness of ILU-smoothing, in: *4th GAMM-Seminar on Robust Multigrid Methods*, ed. W. Hackbusch, Notes on Numerical Fluid Mechanics, Vol. 23 (1988) pp. 217–239.